Cancer Therapy: Preclinical

Clinical Cancer Research

High IGF-IR Activity in Triple-Negative Breast Cancer Cell Lines and Tumorgrafts Correlates with Sensitivity to Anti–IGF-IR Therapy

Beate C. Litzenburger[1,2], Chad J. Creighton[4], Anna Tsimelzon[1], Bonita T. Chan[1], Susan G. Hilsenbeck[1,4], Tao Wang[1,4], Joan M. Carboni[3], Marco M. Gottardis[3], Fei Huang[3], Jenny C. Chang[1,4], Michael T. Lewis[1,4], Mothaffar F. Rimawi[1,4], and Adrian V. Lee[1,4]

Abstract

Purpose: We previously reported an insulin-like growth factor (IGF) gene expression signature, based on genes induced or repressed by IGF-I, which correlated with poor prognosis in breast cancer. We tested whether the IGF signature was affected by anti–IGF-I receptor (IGF-IR) inhibitors and whether the IGF signature correlated with response to a dual anti–IGF-IR/insulin receptor (InsR) inhibitor, BMS-754807.

Experimental Design: An IGF gene expression signature was examined in human breast tumors and cell lines and changes were noted following treatment of cell lines or xenografts with anti–IGF-IR antibodies or tyrosine kinase inhibitors. Sensitivity of cells to BMS-754807 was correlated with levels of the IGF signature. Human primary tumorgrafts were analyzed for the IGF signature and IGF-IR levels and activity, and MC1 tumorgrafts were treated with BMS-754807 and chemotherapy.

Results: The IGF gene expression signature was reversed in three different models (cancer cell lines or xenografts) treated with three different anti–IGF-IR therapies. The IGF signature was present in triple-negative breast cancers (TNBC) and TNBC cell lines, which were especially sensitive to BMS-754807, and sensitivity was significantly correlated to the expression of the IGF gene signature. The TNBC primary human tumorgraft MC1 showed high levels of both expression and activity of IGF-IR and IGF gene signature score. Treatment of MC1 with BMS-754807 showed growth inhibition and, in combination with docetaxel, tumor regression occurred until no tumor was palpable. Regression was associated with reduced proliferation, increased apoptosis, and mitotic catastrophe.

Conclusions: These studies provide a clear biological rationale to test anti–IGF-IR/InsR therapy in combination with chemotherapy in patients with TNBC. *Clin Cancer Res; 17(8); 2314–27. ©2011 AACR.*

Introduction

Despite many advances in the prevention, detection, and targeted therapy of breast cancer, which has resulted in a 30% decline in annual breast cancer death rates since the mid 1990s (1), it is clear that better and more effective breast cancer therapies need to be developed.

Recent molecular classification of breast cancer identified breast cancer subtypes with divergent histopathologic features, clinical outcomes, and therapeutic implications (2). Breast cancer is classified into 2 main subgroups: estrogen receptor alpha (ER) positive and ER negative (3, 4). Triple-negative breast cancers (TNBC) are characterized by low to absent expression of ER, progesterone receptor (PR), and HER2 (5, 6) and account for up to 20% to 25% of all breast cancers. Sixty percent to 90% of TNBCs consist of basal-like breast cancers expressing genes such as cytokeratins *CK5* and *CK14*, which are characteristic of basal epithelial cells (7).

TNBCs currently have no targeted therapies and often respond poorly to chemotherapy (8). They preferentially affect younger women and African American women and are associated with high histologic grade and aggressive clinical behavior (9). TNBCs have high unmet clinical need, and novel targeted therapies need to be discovered.

The insulin-like growth factor (IGF) signaling pathway is a major regulator of growth, survival, migration, and invasion (10, 11). Experimental studies *in vitro* and *in vivo* have provided substantial evidence of a role for IGF-I receptor (IGF-IR) in human breast cancer. Overexpression of a constitutively active IGF-IR or inducible overexpression

Authors' Affiliations: [1]Lester and Sue Smith Breast Center and [4]Dan L Duncan Cancer Center, Baylor College of Medicine, Houston, Texas; [2]Institut für Biochemie und Molekularbiologie, Universitätsklinikum RWTH Aachen University, Aachen, Germany; and [3]Oncology Drug Discovery, Bristol-Myers Squibb Research Institute, Princeton, New Jersey

Note: Supplementary data for this article are available at Clinical Cancer Research Online (http://clincancerres.aacrjournals.org/).

Current address for A.V. Lee: Department of Pharmacology and Chemical Biology, University of Pittsburgh Cancer Institute, Magee Women's Research Institute, 204 Craft Avenue, Pittsburgh, PA 15213.

Corresponding Author: Adrian V. Lee, Department of Pharmacology and Chemical Biology, University of Pittsburgh Cancer Institute, Magee Women's Research Institute, 204 Craft Avenue, Pittsburgh, PA 15213. Phone: 412-641-8554. Fax: 412-641-2458; E-mail: leeav@upmc.edu

doi: 10.1158/1078-0432.CCR-10-1903

Translational Relevance

This study shows that triple-negative breast cancer (TNBC) cell lines and primary tumors exhibit high levels of an insulin-like growth factor (IGF) gene expression signature. Supporting this, cells lines with a high IGF expression signature are especially sensitive to a dual IGF-I receptor (IGF-IR)/insulin receptor (InsR) tyrosine kinase inhibitor (TKI). Treatment of a TNBC tumorgraft with an anti–IGF-IR/InsR dual TKI and chemotherapy resulted in mitotic catastrophe and complete tumor regression. This study provides strong preclincial evidence supporting the investigation of anti–IGF-IR/InsR therapy in combination with chemotherapy in TNBC.

of wild-type IGF-IR in the mouse mammary gland results in rapid mammary tumorigenesis (12, 13). Consistent with this, overexpression of IGF-IR transforms immortalized mammary epithelial cells (MCF10A; refs. 14–16). Clinical studies support the importance of IGFs in breast cancer. In breast cancer specimens, IGF-IR is detected at a very high frequency and levels and activity are increased compared with normal breast (17). High levels of phosphorylated IGF-IR/insulin receptor (InsR) are associated with poor patient prognosis (18). Studies have also shown that elevated levels of serum IGF-I are correlated with increased breast cancer risk (19).

Many preclinical studies targeting the IGF-IR have shown promising antineoplastic activity (17), and early phase 1 (20) and phase 2 (21) reports have been encouraging. Two predominant targeted strategies to inhibit IGF-IR function are in the development phase: monoclonal antibodies, which are highly specific for the IGF-IR and cause downregulation of the receptor, and tyrosine kinase inhibitors (TKI), which are ATP-competitive inhibitors of the IGF-IR and InsR tyrosine kinase domains (22).

An important outstanding question in the clinical development of anti–IGF-IR therapy is to identify appropriate patient populations, allowing specific treatment of patients whose tumors show dependence to this pathway for continued survival and proliferation. Many studies showed that both *IGF-IR* and its downstream adaptor *IRS1* are estrogen-regulated genes (23). Furthermore, IGF-I can activate the ER (24). This bidirectional positive feedback supported the concept of targeting both ER and IGF-IR in breast cancer, and many clinical trials are currently testing this strategy (25–27). However, there is also evidence for a role for IGF-IR in TNBC. A number of tumor suppressor genes such as *p53* and *BRCA1* represses the *IGF-IR* promoter. Mutations in these tumor suppressor genes in TNBC are associated with elevated IGF-IR levels (28). Furthermore, IGF-IR is amplified in basal breast cancer (29), and high levels of IGF-IR protein are seen in basal breast cancers (30).

In this study, we show that IGF activity, as measured by a gene expression signature, is activated in TNBC patient tumors and cell lines in culture. This high level of the IGF signature correlates with sensitivity to a new dual IGF-IR/InsR small molecule inhibitor, BMS-754807. Consistent with this, BMS-754807 alone is effective at causing growth inhibition of a TNBC tumorgraft and, in combination with chemotherapy, results in tumor eradication. This preclinical study provides substantial support and rationale for a clinical trial using inhibitors against IGF-IR in combination with chemotherapy in TNBC.

Methods

BMS-754807

The chemical structure of BMS-754807 and its activity against IGF-IR has been recently described (31). For *in vitro* studies, BMS-754807 was dissolved in DMSO to give a 10 mmol/L solution. For *in vivo* studies, BMS-754807 was formulated in PEG400:H_2O (80:20).

Cell culture

Breast cancer cell lines were obtained from American Type Culture Collection, except H3396, which was obtained from the Pacific Northwest Diabetes Research Institute (Seattle, WA). The MCF-7/HER2 cell line was made by stable transfection of the *HER2* gene into MCF-7 cells. Cells were grown using the recommended culture conditions according to Neve and colleagues (32). Of note, the cell lines used to test the IC_{50} of BMS-754807 did not require insulin to be added to the medium. MCF10A cells were cultured in DMEM/F12 medium supplemented with 5% horse serum, 20 ng/mL epidermal growth factor, 10 μg/mL insulin, 0.5 μg/mL hydrocortisone, 100 ng/mL cholera toxin, and 100 units/mL penicillin-streptomycin. SUM breast cancer cell lines also required the addition of insulin.

Monolayer growth assay

For breast cancer cell line studies, cells were plated at 1,000 to 12,000 cells per well, depending on the growth properties of each cell line in 96-well microtiter plates and incubated overnight. The next day, the start absorbance (cell number at the beginning of the experiment, i.e., at time of drug addition), was measured in which no compound was added and the plate was immediately developed by the method described in the following text. BMS-754807 was serially diluted and added. After 72-hour exposure, cell viability was determined by MTS assay (Promega). Percentage of cell growth inhibition was calculated as % of control = (End absorbance – Start absorbance) × 100%. The growth curves (expressed as a percentage of growth observed in untreated controls) were used to determine the IC_{50} value, which is the drug concentration at which 50% of maximal growth inhibition was observed.

Comparative gene expression analysis

Comparative gene expression analysis was carried out by determining genes with significantly different expression between sensitive cell lines with an IC_{50} value of less than 4 μmol/L ($n = 10$) and resistant cell lines with an IC_{50} value

of greater than 14 μmol/L ($n = 9$) by using dChip software (33, 34). We utilized publicly available gene expression data published by Neve and colleagues (32). Differentially expressed genes were found using *t* test. FDR was estimated by permutation method. We used $P = 0.001$, which resulted in 136 differentially expressed probe sets representing 114 genes, with FDR of less than 5%. Hierarchical clustering and expression values were visualized as heat maps.

To assign cell lines to breast cancer subtypes, we scored the cell lines for subtype, essentially as previously described by using the data set from Hoadley and colleagues (35). In brief, for each gene common to the Hoadley platform and the other breast-array data set platform, we computed the mean centroid of the subtypes in the Hoadley data set and centered each group average on the centroid. We then took the Pearson correlation (using all genes common to both array data sets) between the Hoadley-centered averages and the expression values of each profile in the independent data set.

RNA isolation and quantitative real-time PCR

To validate the comparative gene expression analysis, 7 sensitive and 6 resistant cell lines were cultured in triplicates. The sensitive cell lines MCF-7, BT20, MDA-MB-468, HS758T, MDA-MB-231, HCC38, and MDA-MB-436 and the resistant cell lines ZR75-1, SKBR3, BT474, CAMA-1, MDA-MB-134, and UACC812 were used. RNA was isolated using RNeasy mini kit (QIAGEN). mRNA was converted to cDNA in a final volume of 100 μL, using 0.5 μg RNA, 0.5 μL random primers, and 25 mmol/L desoxynucleotide triphosphate. After the samples were heated for 5 minutes at 65°C, 20 μL of 5× first-strand buffer (Invitrogen), 5 μL 0.1 mol/L dithiothreitol, and 0.5 μL of Superscript II RNase H reverse transcriptase (Invitrogen) were added. Reverse transcription was carried out at 25°C for 5 minutes, 48°C for 30 minutes, and 70°C for 10 minutes. Quantitative reverse transcriptase PCR analysis was carried out with the following primers: Cav2-fwd, 5′-ATCCCCACCGGCTCAACT; Cav2-rev, 5′-CCGGCTCTGCGATCACAT; Cav1-fwd, 5′-GGTCAACCGCGACCCTAAA; Cav1-rev, 5′-CCTTCCAAATGCCGTCAAA; Spdef-fwd, 5′-TGGATGAAAGAGCGGACTTCA; Spdef-rev, 5′-TCGGTCCAGCTCTCCTCACT; ErbB3-fwd, 5′-CGGTTATGTCATGCCAGATAC; ErbB3-rev, 5′-GAACTGAGACCCACTGAAG AAAGG. qRT-PCR was carried out in a ABI Prism 7900 sequence detector, using the Power SYBR Green PCR Master Mix (Applied Biosystems). Each reaction contained 5 μL of template cDNA, a final concentration of 0.15 μmol/L forward and reverse primer, 12.50 μL of 2X SYBR Green Buffer and RNAse-free H_2O to make a final volume of 25 μL. The PCR was carried out at 50°C for 2 minutes, denaturing at 95°C for 10 minutes, 40 cycles of 95°C for 15 seconds, and 60°C for 30 seconds. Analysis was done using the ΔΔCt method, normalizing first to the average of the housekeeping β-*actin*. The expression values were $\log_{10}$ transformed; graphs were represented as the mean and error bars represent the SEM. Data points were compared using a 2-tailed *t* test.

Immunohistochemistry

A tissue microarray (TMA) was generated for immunohistochemical analysis. To account for cancer tissue heterogeneity, 0.6-mm inch diameter cores were punched from regions selected on the original tumor slides by H&E to include all patterns of differentiation. The TMA was sectioned at 5 μm onto Superfost Plus slides (Fisher Scientific), deparaffinized, and rehydrated using a Shandon-Lipshaw Varistain (program 2). Subsequently, slides were stained with H&E and then examined microscopically by a pathologist. IHC was carried out after heat-induced, citrate-based antigen retrieval for p-IGF-IR/Y1161 (Abcam; ab39398-100), BrdU, CC3 (Covance), and Ki67 (Dako), using a Vectastain ABC peroxidase immunodetection kit. Slides were counterstained with hematoxylin, dehydrated, and mounted using cytoseal. IHC for total IGF-IR (Ventana) was carried out on the Ventana Benchmark XT according to the manufacturer's protocol. Images were taken with a Nuance camera at magnification of 20× and 40×.

Immunoblot analysis

Human tumorgraft tissues were lysed by electric homogenizer for 8 seconds in lysis buffer [1% Triton X-100, 50 mmol/L HEPES (pH 7.4), 150 mmol/L NaCl, 1.5 mmol/L $MgCl_2$, 1 mmol/L EGTA, 100 mmol/L NaF, 10 mmol/L NaPPi, 10% glycerol, 1 mmol/L Na_3VO_4, and protease inhibitor (Roche Applied Science)] and incubated on ice with occasional shaking for 20 minutes. The supernatant was collected by centrifugation at 14,000 rpm, 4°C for 10 minutes and quantified by BCA protein assay (Pierce). Total protein extract (50–75 μg) was resuspended in denaturing sample loading buffer, separated by 8% SDS-PAGE, and transferred to a nitrocellulose membrane overnight at 4°C. The membrane was blocked with PBS plus 0.05% Tween-20 (PBST) containing 5% bovine serum albumin for 1 hour. The following antibodies were utilized: anti–phospho-IRS1 (Tyr612,44-816G; Biosource, 1:500), anti-IRS1 (#sc-7200; Santa Cruz Biotechnology, 1:500) anti–phospho-IGF-IR/InsR (Tyr1135/1136, #3024; Cell Signaling Technology, 1:500), anti–IGF-IRβ (#sc-713; Santa Cruz Biotechnology, 1:500), anti–phospho-ERK1/2 (#9101; Cell Signaling Technology, 1:1,000), anti-ERK1/2 (#06-182; Upstate/Millipore, 1:1,000), anti–phospho-AKT (Ser473, #9271; Cell Signaling Technology, 1:1,000), anti-AKT (#9272; Cell Signaling Technology, 1:1,000), and anti–β-actin (#A1978; Sigma, 1:4,000). Antibodies were incubated in blocking solution for 4 hours. Subsequently, the membrane was washed 3 times with PBST for 5 minutes and then incubated with a horseradish peroxidase–linked secondary antibody (Amersham Pharmacia Biotech) at a dilution of 1:4,000 in blocking solution. Bands were visualized by enhanced chemiluminescence (Pierce Biotechnology) and captured using an Alpha Innotech 7000 imager (Alpha Innotech).

Tumorgraft study

All procedures were conducted in accordance with the NIH *Guide for the Care and Use of Laboratory Animals* and

were approved by the Institutional Animal Care and Use Committee of Baylor College of Medicine. Human breast tumors were obtained as core biopsies or pieces of tumors after surgery and implanted in humanized cleared fat pads of NOD/severe combined immunodeficient (SCID) mice for establishing human tumorgrafts. Tumorgraft lines are maintained by transplantation of small pieces (1 mm^3) of tumorgraft into 4- to 6-week-old female NOD/SCID mice (Harlan Sprague-Dawley Inc.). When tumorgrafts reached 1 cm^3, they were then retransplanted. For the testing the efficacy of BMS-754807 with and without chemotherapy, 4- to 6-week-old female NOD/SCID mice were transplanted with a 1-mm^3 piece of tumorgraft into a cleared number 4 mammary fat pad. Tumor volume (in mm^3) was measured weekly with a digital caliper according to the formula for an ellipsoid sphere: (long dimension) $\times$ (short dimension)^2/2. When tumors reached a volume between 100 and 200 mm^3, they were randomized to receive the following treatments: vehicle, 50 mg/kg BMS-754807 daily by oral gavage, 20 mg/kg docetaxel weekly by intraperitoneal injection, or the combination of 50 mg/kg BMS-754807 daily and 20 mg/kg docetaxel weekly by intraperitoneal injection. Tumor volume and body weight were measured daily. All mice were sacrificed when control tumors reached 1,000 mm^3. Plots of tumor growth curves and body weight measurements were generated using GraphPad Prism (GraphPad Software, Inc.).

Measurement of serum glucose

Whole blood from mice was collected 3 hours after the final treatment with single agents or combination of BMS-754807 and docetaxel, inserted into BD microtainer serum separator tubes (VWR; #VT365956), and allowed to clot at room temperature for 1 hour. Samples were then centrifuged for 7 minutes at 12,000 rpm. The top layer containing the serum was collected from each tube and stored at $-80°C$. Serum glucose was measured using a glucose assay kit (BioVision). Samples (1 μL) were diluted in supplied assay buffer and tested in duplicate by using the protocol provided by the supplier. Serum glucose level was measured from the standard curve of the supplied glucose-positive control. Standard deviation was calculated using the duplicate values in the assay.

Measurement of serum insulin

Serum samples were stored at $-80°C$ and thawed on ice before being tested. Serum insulin was measured using the Ultra Sensitive Mouse Insulin ELISA Kit (Crystal Chem, Inc.). Samples (0.5 and 1 μL) were diluted in kit supplied assay diluent and tested in duplicate. Vendor-supplied assay protocol was followed, and insulin concentration was measured from the standard curve of the supplied insulin standard. SD was derived from the duplicate samples.

IGF signature *t*-score

To score each breast cancer cell line within a set for similarity to the IGF gene signature, a "*t*-score" for each breast cancer cell line in relation to the IGF gene signature was derived, which was similar to previously published analyses (36). The *t*-score was defined as the 2-sided *t*-statistic comparing the average of the IGF-induced genes with that of the IGF-repressed genes within each breast cancer cell line. The gene expression values in the breast cancer cell line data set ($n = 51$ breast cancer cell lines; ref. 32) were first normalized to the median before computing the *t*-score. For each gene transcription profile data set, we assigned intrinsic molecular subtypes to the cell lines, essentially as previously described (37), using the human tumor data set from Hoadley and colleagues (35) to define the subtype-specific expression patterns.

Statistical methods

To compare the tumor growth pattern among the treatment groups in the tumorgraft study, data were analyzed by a mixed model with treatment group, polynomial terms of day up to the third order, interactions as fixed effects, and subject as a random-effect factor. Tumor volumes at day 14 were then compared pairwise among the groups by using model-based contrasts. The overall growth curves were also compared by examining the interaction terms in the model. ANOVAs and pairwise comparisons with Holm adjustment for multiple comparisons were done for comparisons of glucose and insulin levels, BrdU, Ki67, and CC3 between the 4 groups: vehicle, BMS-754807, docetaxel, and combination. To achieve normality, log transformation was used for glucose and insulin data; Arcsine square-root transformation was used for BrdU, Ki67, and CC3 data because data were expressed as proportion from 0 to 1.

Results

An IGF gene expression signature is present in TNBC

We previously reported the development of an "IGF-I gene signature" consisting of a pattern of genes up- or downregulated by IGF-I (36). We found that this IGF signature was present in human breast cancers, specifically the subtypes luminal B and TNBC (36). To independently validate these results, we analyzed the IGF gene signature in a recently published data set of 198 node-negative breast cancers (38) and confirmed the presence of the IGF signature in the majority of ER-negative tumors (Supplementary Fig. S1A). We went on to apply the IGF signature to a more recent profile data set from Hoadley and colleagues (35). This independent cohort of 248 tumors was previously classified into breast cancer subtypes by using an intrinsic gene expression signature. The IGF gene signature was present in most basal tumors, luminal B tumors, and a subset of HER2-positive tumors (Supplementary Fig. S1B) compared with other subtypes. These data suggest that the IGF signature is present in TNBC and that these tumors may be candidates for anti–IGF-IR therapy.

The IGF gene expression signature is reversed by anti–IGF-IR inhibitors

We next set out to examine the effect of IGF-IR inhibitors on the IGF signature. We reasoned that regulation of genes

by IGF-I (which made up the IGF gene signature) should be reversed by anti–IGF-IR inhibitors. Consistent with this, when we examined the levels of genes that we previously found to be induced or repressed by IGF-I in neuroblastoma xenografts treated with an anti–IGF-IR (h10H5; Genentech) antibody (39), there was a striking reversion in their levels (Fig. 1A). Thus, genes induced by IGF-I in MCF-7 cells were repressed by h10H5 treatment of the neuroblastoma xenograft and genes repressed by IGF-I were now induced. This result was highly significant ($P \approx 0$). Results were highly similar to those obtained with an IGF-IR/InsR TKI (A-928605; Abbott; ref. 40) that was administered *in vitro* to NIH3T3 fibroblasts transfected with the IGF-IR (Fig. 1B). Finally, we generated gene expression data from colon cancer xenografts (GEO) grown *in vivo* and then treated with an anti-IGF TKI (BMS-754807, 12.5 mg/kg/d) for various time points of 1, 6, and 24 hours and 15 days. Treatment of these GEO xenografts resulted in gene expression values that were again reversed compared with the IGF signature (Fig. 1C). Note that there was no change in the IGF signature after 1 hour, but after 6 hours of exposure to the drug, a strong reversion of the IGF signature was seen, which is entirely consistent with the pharmacodynamics and pharmacokinetics of BMS-754807. These data give us confidence that our signature can measure IGF activity and, furthermore, suggest that the IGF signature might indicate cells that have an active IGF pathway and thus may respond to an IGF-IR inhibitor.

When we originally developed the IGF signature, we attempted to reduce the importance of proliferative genes by (i) including only those genes that are modulated by IGF-I at both 3 and 24 hours, (ii) removing genes annotated as being associated with proliferation in Gene Ontology (GO), and (iii) removing genes that were found to be induced in fibroblasts stimulated to proliferate by serum (41). In our previous report, we confirmed that the IGF signature does not correlate with the proliferative rate of cell lines (41). Thus, this reversal of the signature by IGF-IR inhibitors (Fig. 1) presumably does not simply reflect changes in cell growth but rather highlights changes in metabolism and DNA repair (the major GO term-defined classes of genes represented in the IGF gene signature). To further examine the specificity of the IGF signature, and its reversion, we examined the levels of genes in the IGF signature on a data set of ovarian cancer cells (36M2) treated with chemotherapy (carboplatin). Importantly, chemotherapy had no discernable effect upon the IGF gene signature; indeed, it weakly induced the IGF signature, perhaps due to a DNA damage response (Supplementary Fig S1D).

A recent study comparing genes regulated by growth factors [IGF-I, insulin, epidermal growth factor (EGF), and heregulin] in MCF-7 cells showed that there was a highly significant overlap (42), consistent with highly redundant nature of growth factor downstream signaling [e.g., phosphoinositide 3-kinase, extracellular signal regulated kinase (ERK) 1/2]. We therefore examined whether the IGF-I signature would be modulated by inhibition of other growth factor receptors. We developed gene expression profiles from colon cancer (GEO) xenografts treated for various lengths of time with the EGF receptor inhibitor Erbitux (cetuximab; 1 mg/kg every 3 days). Interestingly, the IGF signature was reversed by Erbitux, indicating that the IGF signature is likely a marker of active growth factor signaling and highlights pathways downstream of receptor TKIs (Supplementary Fig. S1C).

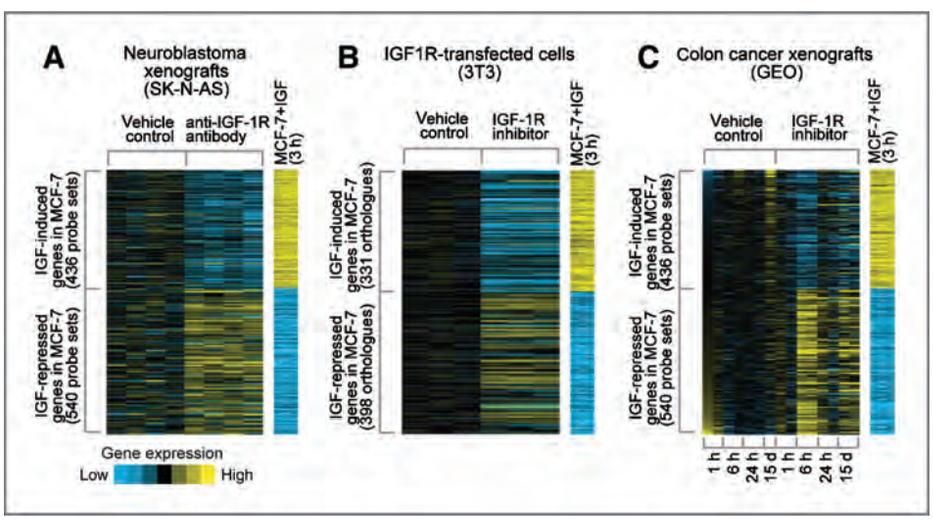

Figure 1. An IGF gene signature is reversed by treatment of cancer xenografts and IGF-IR–overexpressing NIH3T3 fibroblasts with anti–IGF-IR inhibitors. Genes in the IGF-I gene signature derived from MCF-7 cells stimulated with IGF-I (31) were examined. A, a gene expression profile of neuroblastoma (SK-N-AS) xenografts treated with vehicle or an anti–IGF-R antibody. B, IGF-IR–transfected NIH3T3 fibroblasts treated with an IGF-IR small molecule inhibitor. C, colon cancer xenografts treated with the small molecule inhibitor BMS-754807. For A–C, relative gene expression is represented using a yellow-blue color scale; patterns for genes that are upregulated (yellow) in the IGF gene signature are separate from the patterns for genes that are downregulated (blue).

Triple-negative/basal-like breast cancer cell lines show activation of the IGF gene signature

To examine whether the IGF gene signature is associated with response to inhibition of IGF-IR/InsR, we studied cell lines grown in culture, where one can rapidly assess response. Therefore, we examined the IGF-I gene signature in a publicly available data set of gene expression profiles from a large panel of breast cancer cell lines (32). Figure 2A shows a panel of breast cancer cell lines arranged according to their intrinsic subtype (as defined using the Hoadley data set; ref. 32). The IGF signature is present in the majority of basal-like (and TNBC) breast cancer cell lines. We assigned each cell line a *t*-score based on the similarity of its gene expression profile to the IGF signature and the positive *t*-score in the majority of TNBC cell lines highlights the presence of the signature in this subtype (Fig. 2B). These data are entirely consistent with Figure S1 and our previous report of the IGF signature in TNBC (36), suggesting that the IGF-IR pathway is highly active in the triple-negative/basal-like subtype of breast cancer.

An IGF-IR TKI, BMS-754807, shows selective activity in TNBC cell lines

To test whether the presence of the IGF signature in triple-negative/basal-like breast cancer cell lines was associated with response to an IGF-IR/InsR inhibitor, the sensitivity of a new dual IGF-IR/InsR TKI (BMS-754807) currently in phase 1/2 clinical trials was determined by MTS assay in a panel of 30 breast cancer cell lines. Among the different tumor cell lines, sensitivity presented as IC_{50} to BMS-754807 varied widely from 0.1 to 25 μmol/L (Fig. 3A). When defining cell lines as sensitive or resistant on the basis of the median IC_{50} value (6.4 μmol/L), we found a clear correlation between the sensitive/resistant classification to BMS-754807 and specific breast cancer subtypes. Figure 3A shows that the greatest response to BMS-754807 was in triple-negative/basal-like breast cancer cell lines (10/15) whereas luminal breast cancer cell lines and HER2-overexpressing cell lines were relatively resistant (13/15). Compared with all cell lines, the TNBC group was enriched for cell lines with low IC_{50}. Importantly, when the IC_{50} is plotted against the *t*-score for the IGF gene signature for each cell line, there is a significant inverse correlation ($r = -0.41$, $P = 0.014$), with a higher *t*-score (indicating an active IGF pathway) being associated with a greater response (lower IC_{50}) to BMS-754807 (Fig. 3B). These data strongly suggest that BMS-754807 is active in TNBC.

One hundred fourteen differentially expressed genes identify TNBC cell lines as most responsive to BMS-754807

To examine genes and pathways associated with response to BMS-754807, we carried out comparative gene expression analysis between the 10 most sensitive cell lines with an IC_{50} value below 4 μmol/L BMS-754807 and the 9

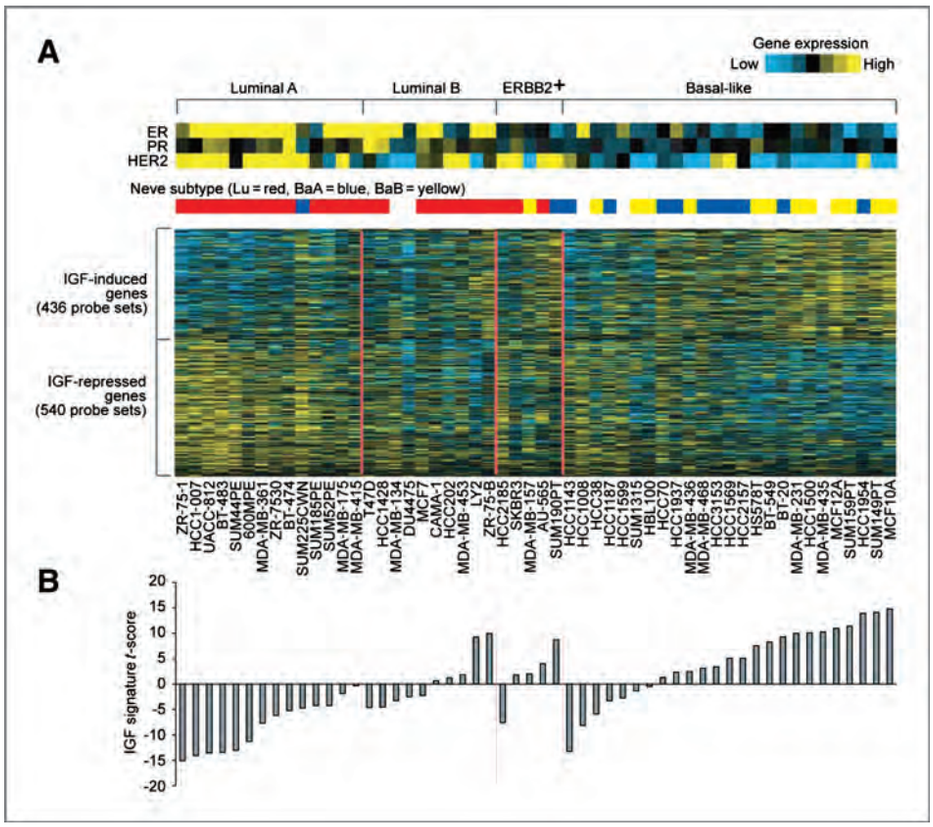

Figure 2. IGF gene signature is present in triple-negative/basal-like breast cancer cell lines. Breast cancer cell line profiles were classified using the Hoadley data set, in which intrinsic subtypes were previously defined. The correlation was computed between a given cell line gene expression profile and the mean centroid of each subtype; cell lines were then assigned to a subtype with the highest correlation. A, the heat map represents the IGF gene signature in the cell lines according to subtype. ER, PR, and HER2 mRNA levels are shown. In addition, the breast cancer subtype is indicated as defined in the original gene expression study by Neve and colleagues (32). B, the graph represents the *t*-score for each cell line, based on the similarity to the IGF signature.

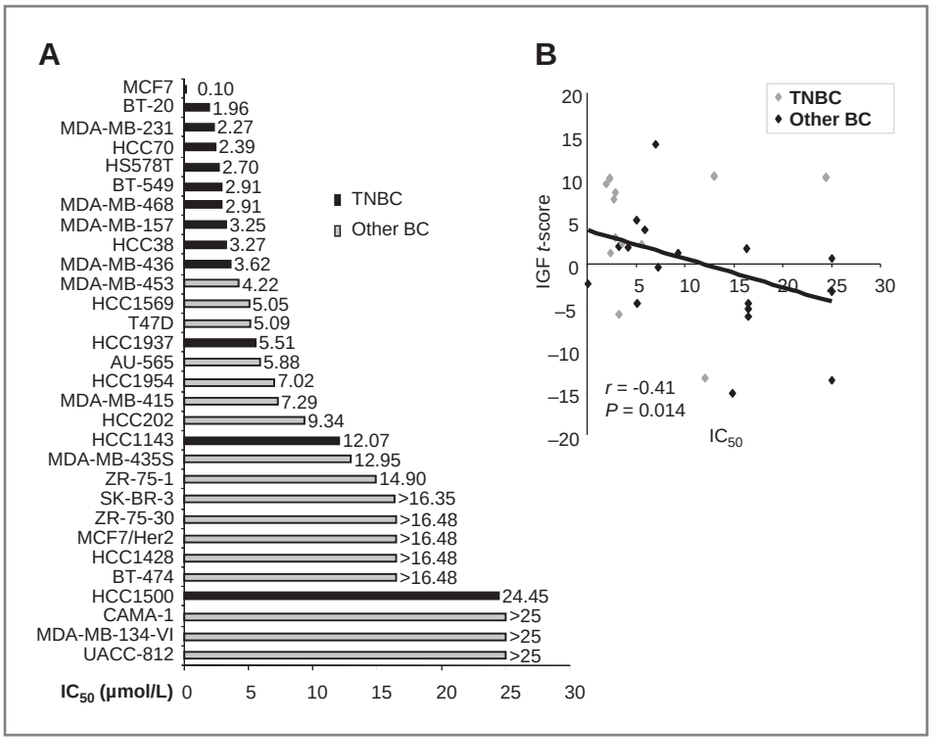

Figure 3. BMS-754807 is active in triple-negative/basal-like breast cancer (BC) cell lines. A, the concentration of BMS-754807 required to reduce growth by 50% (IC_{50}) was calculated for each cell line by using monolayer proliferation and MTS assay. Breast cancer cells were seeded at 1,000 to 12,000 cells per well depending on the cell line in 96-well microtiter plates and incubated overnight. BMS-754807 was serially diluted and added. After 72-hour exposure, MTS assay was carried out. Bars represent the average IC_{50} (μmol/L) of each breast cancer cell line. For 7 cells lines the IC_{50} was not reached (16.49 and 25 μmol/L, respectively). Sensitive cell lines have an IC_{50} below the mean of the group of cells (6.4 μmol/L); resistant cell lines are above the mean. The graph shows cell lines ranked according to its IC_{50}. Black bars represent cell lines that have a basal-like gene expression signature (TNBC) based on the studies of Neve and colleagues (38) and gray bars represent luminal or HER2-positive cell lines. B, IC_{50} is plotted alongside the *t*-score for the IGF signature for each cell line. Pearson correlation shows there is a significant correlation ($r = -0.41$, $P = 0.014$), with a higher *t*-score (indicating an active IGF-IR pathway), being associated with a greater response (lower IC_{50}) to BMS-754807.

most resistant cell lines with an IC_{50} value above 14 μmol/L BMS-754807 using gene expression data published by Neve and colleagues (32). As predicted from Figure 3B, these 2 panels of cell lines showed a statistically different IGF *t*-score (sensitive, 3.59 ± 1.64; resistant, -3.91 ± 2.57; $P < 0.05$). Comparative gene expression analysis between these 2 sets of cell lines identified 136 probe sets corresponding to 114 genes [$P < 0.001$; false discovery rate (FDR) < 5%] that were differentially expressed between sensitive and resistant cell lines. The top 10 differentially expressed genes were validated in a panel of 7 sensitive and 6 resistant breast cancer cell lines by quantitative reverse transcriptase (RT)-PCR (qRT-PCR; Supplementary Fig S2). We analyzed the 114 genes in a panel of 51 breast cancer cell line profiles with known and unknown IC_{50} values to BMS-754807 (32). Hierarchical clustering separated the cells lines into 2 major bins: ER-negative cell lines that were sensitive and ER-positive cell lines that were mostly resistant (Fig. 4A).

We found that there was significant overlap between the 114 genes (136 probe sets) and the IGF signature developed from MCF-7 cells. Thus, of 66 probe sets with an increase in sensitive cell lines, 13 were increased in the IGF signature [from a total of 436 (one-sided Fisher's exact test, $P = 4.E\text{-}10$)]. Of the 70 probe sets with a decrease in sensitive cell lines, 7 were also decreased in the IGF signature from a total of 540 probe set (one-sided Fisher's exact test, $P = 0.002$).

Consistent with the IGF signature being present in TNBC and correlating with sensitivity to an IGF-IR inhibitor, when we examined the levels of the 136 probe sets in human breast cancers, we found enrichment in TNBC (Fig. 3B). When examining tumors subtyped according to Hoadley and colleagues, we found 114 genes enriched in basal, claudin-low, normal, and a subset of HER2-positive tumors. The patterns of enrichment of the 136 probe sets (114 genes) strongly resembled the patterns seen with the IGF signature (Supplementary Fig. S1). We identified that many of these 114 genes were actually markers of the basal or luminal subtype, with sensitive cell lines expressing basal markers such as CAV1 and CAV2 whereas resistant cell lines expressed luminal markers such as ErbB3 and SPDEF (Supplementary Fig. S2).

To examine the clustering data further, we determined the sensitivity to BMS-754807 of breast cancer cell lines with an

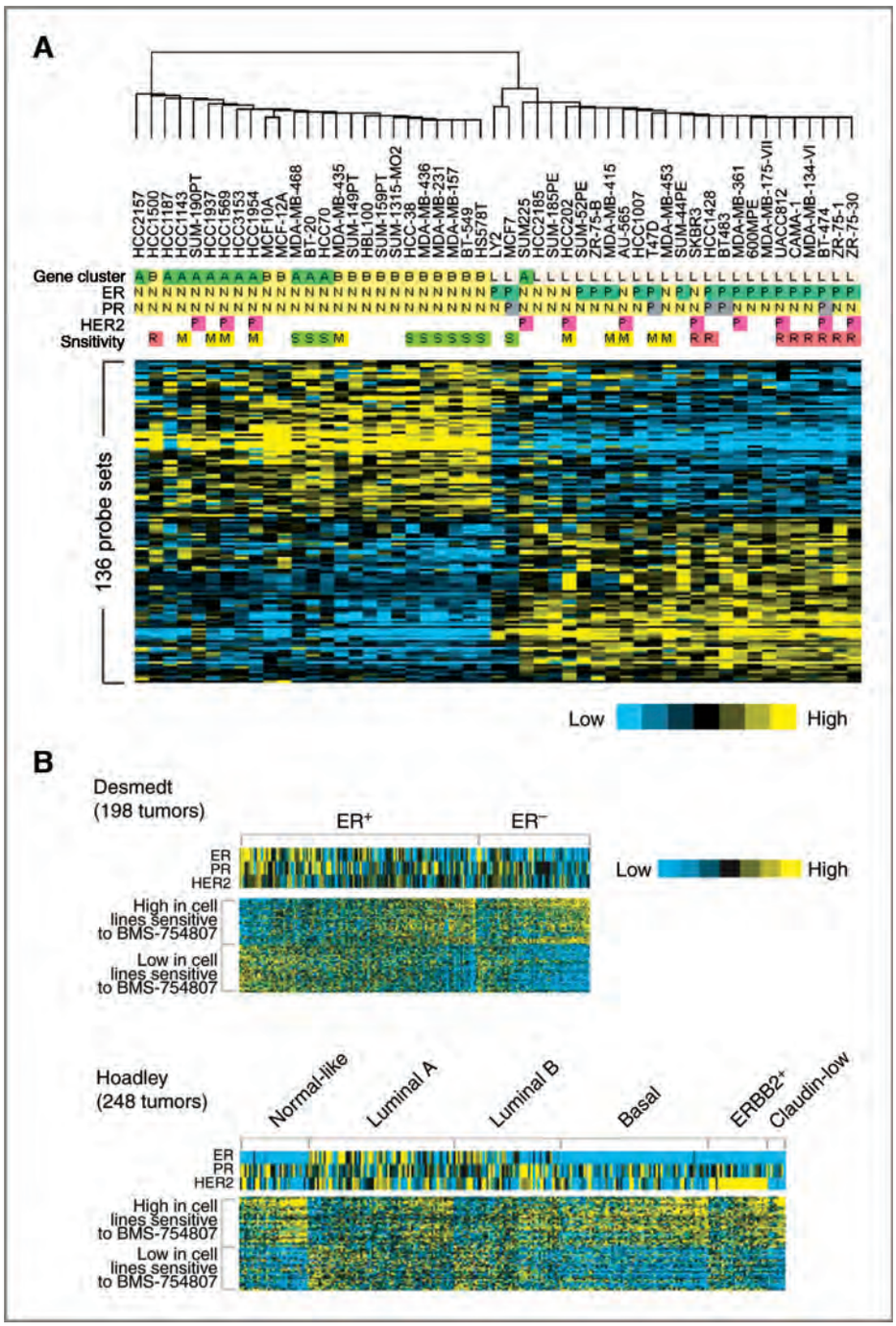

Figure 4. One hundred fourteen differentially expressed genes identified TNBC cell lines as most responsive to BMS-754807. A, 136 differentially expressed probe sets, representing 114 genes, were analyzed in 51 breast cancer cell line profiles published by Neve and colleagues (32), with known and unknown IC_{50}. S, sensitive (IC_{50} < 4 μmol/L); M, medium (IC_{50} = 4 μmol/L < 14 μmol/L); R, resistant (IC_{50} > 14 μmol/L). In addition, the ER, PR, and HER2 status is indicated (P, positive; N, negative). Gene cluster indicates the breast cancer subtype as defined in the original gene expression study by Neve and colleagues (A, basal A; B, basal B; L, luminal). B, 136 differentially expressed probe sets, representing 114 genes, were analyzed in 2 published data sets of clinical breast tumors from Desmedt and Hoadley. Within the ER-positive and ER-negative, as well as the distinct breast cancer subtype, tumors are ordered from those with the least similarity to the 114-gene signature pattern to those with the highest similarity to the 114-gene signature.

unknown IC_{50} value by MTS assay. Among the cell lines tested, the TNBC cell lines SUM149PT and MCF10A showed the greatest response to BMS-754807 whereas cell lines that are ER negative but overexpress HER2 (SUM225 and SUM190PT) are less sensitive to BMS-754807 (Fig. 4B). Luminal breast cancer cell lines such as ZR75B, MDA-MB-175VII, and MDA-MB-316 showed the least response to BMS-754807. It is interesting to note that the sensitive cell lines required insulin for regular growth, whereas the resistant cells are routinely grown in the absence of insulin. This may highlight the growing evidence for a role for insulin in breast cancer, which is being studied by many groups.

Novel tumorgraft models of human TNBC show strong activation of IGF-IR/InsR

Preclinical cancer research has relied heavily on cell lines grown in culture and then xenografted for growth in mice. However, recent work has shown that human cancer cells placed directly into the mouse (tumorgrafts) may be a more appropriate model that is better at predicting response to drugs in humans (43). We have recently developed several new tumorgraft models of human TNBC. We screened 7 TNBC tumorgrafts for activity of the IGF-IR and InsR by both immunohistochemistry (IHC) and immunoblotting (IB). Figure 5A shows 3 representative tumorgrafts that express various levels of IGF-IR protein and have divergent levels of active phosphorylated pY-IGF-IR/InsR (antibodies are only available for those which detect both pY-IGF-IR and pY-InsR together). We generated gene expression data from the tumorgrafts and calculated an IGF signature *t*-score for each tumorgraft. Analysis of these profiles showed that tumorgraft MC1 (44) had the highest level of IGF-IR and pY-IGF-IR/InsR and, in addition, had a high IGF signature *t*-score. Protein lysates from the same tumorgrafts as shown in Figure 5A confirmed that MC1 had the highest activation of IGF-IR/InsR (Fig. 5B). Activation of downstream signaling molecules varied among the tumorgraft models. MC1 had high levels of IRS1 and activated AKT, whereas the tumorgraft 2665A showed activation of MAPK.

BMS-754807 inhibits growth of MC1 TNBC tumorgrafts and, when combined with chemotherapy, causes complete regression

Our studies identified TNBC and TNBC cell lines as having an active IGF pathway. As we have previously shown that BMS-754807 is most active in TNBC cell lines *in vitro*, we directly examined the effectiveness of the dual IGF-IR/InsR inhibitor BMS-754807 in the MC1 tumorgraft model of TNBC alone as a single agent or in the presence of chemotherapy (docetaxel). We chose the tumorgraft MC1 for this preclinical study, as it showed the highest levels of active and total IGF-IR and also a high IGF *t*-score (Fig. 5). A recent study examining timing of anti–IGF-IR therapy and chemotherapy in cells in culture showed that most efficacious combination was chemotherapy followed by anti–IGF-IR therapy (45). We thus administered docetaxel followed by BMS-754807 the next day. Single-agent BMS-754807 achieved a statistically significant ($P < 0.001$) reduction in tumor growth when compared with the control group (Fig. 6A). Docetaxel stabilized MC1 tumor growth. Strikingly, combined treatment with BMS-754807 and docetaxel showed superior tumor growth inhibition to either single agent alone ($P < 0.001$), and 4 of 6 mice receiving the combined agents had tumors regression until no tumor was palpable.

To confirm the ability of BMS-754807 to inhibit IGF-IR activity in TNBC, tyrosine phosphorylation and total levels of IGF-IR/InsR were examined in the various treatment groups. Both pY-IGF-IR/InsR and IGF-IR showed membrane staining with a small amount of cytoplasmic staining (Fig. 6B). There was no change in the levels of pY-IGF-IR/InsR between tumors treated with docetaxel and vehicle (Fig. 6B). In contrast, BMS-754807 completely blocked IGF-IR/InsR phosphorylation. There was no change in levels of total IGF-IR between the different treatment groups.

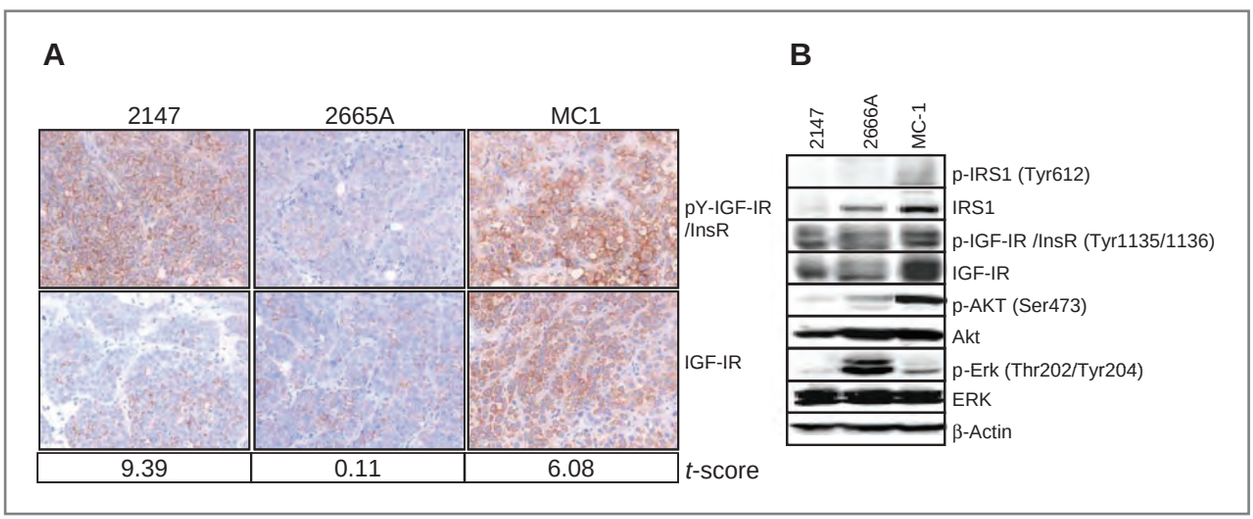

Figure 5. TNBC tumorgrafts express high levels of active IGF-IR. A, 3 different TNBC tumorgraft lines (2147, 2665A, and MC1) were harvested and processed in paraffin. IHC was carried out on 5-μm sections for anti–pY-IGF-IR (phospho-IGF-IR) and total IGF-IR. Microarray analysis was carried out on these tumorgrafts. On the basis of the gene expression data, an IGF signature *t*-score was calculated for each tumorgraft as indicated underneath the representative photograph. B, the same 3 tumorgraft lines were lysed and analyzed by immunoblotting and probed using IGF-IR–specific antibodies as well as total/phospho-specific antibodies for IRS1, AKT, and ERK1/2. β-Actin was used as a loading control. Tumorgraft lines that were not relevant to this study were cropped out between 2665A and MC1.

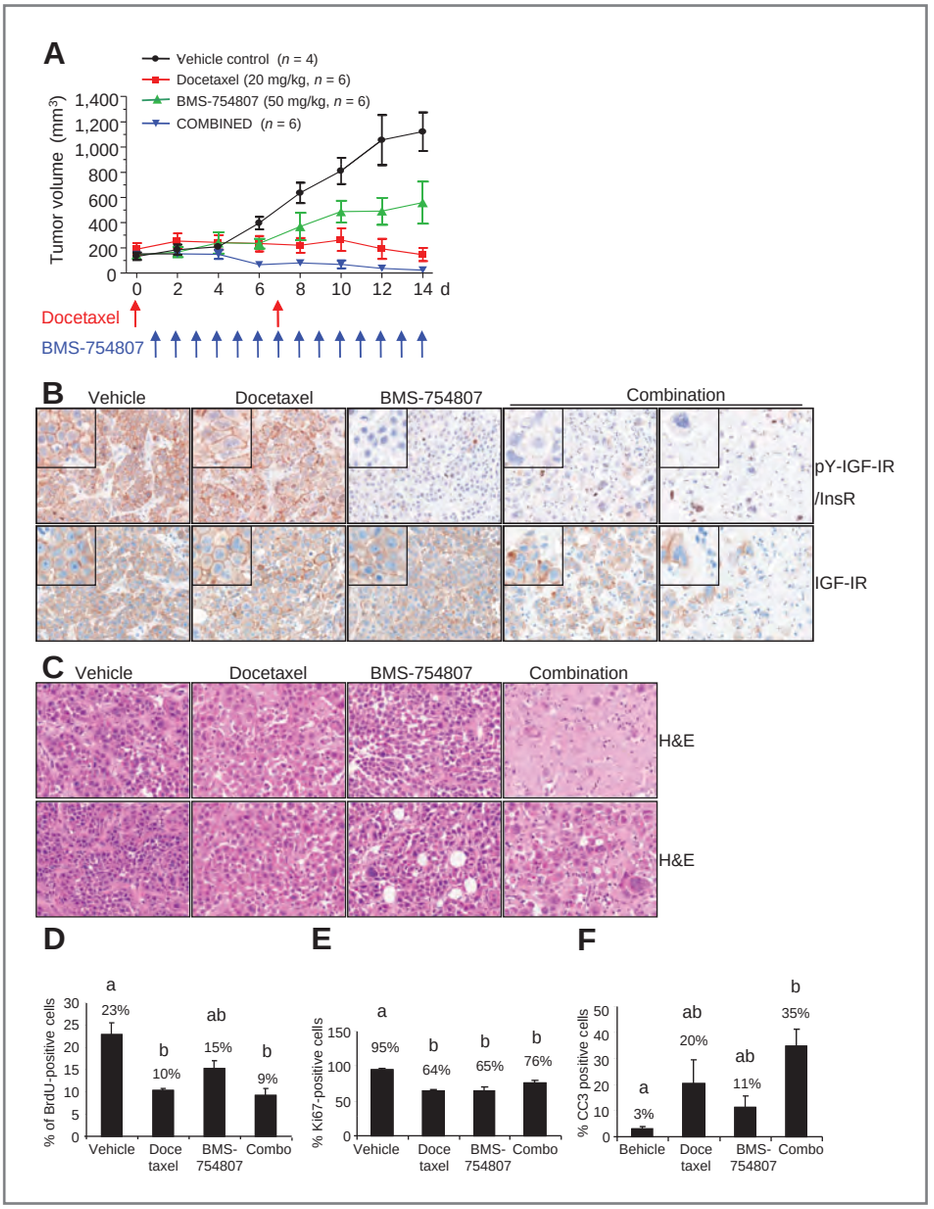

Figure 6. BMS-754807 inhibits growth of TNBC tumorgrafts and causes regression in combination with chemotherapy. A, 4- to 6-week-old female NOD/SCID mice were transplanted with a 1-mm^3 piece of tumorgraft into a cleared number 4 mammary fat pad. When tumors reached a volume between 100 and 200 mm^3, they were randomized to receive the following treatments: vehicle, 50 mg/kg BMS-754807 daily by oral gavage, 20 mg/kg docetaxel weekly by intraperitoneal injection, or the combination (Combo) of 50 mg/kg BMS-754807 daily and 20 mg/kg docetaxel weekly by intraperitoneal injection. Tumor volume and body weight were measured daily. B, untreated and treated tumors were processed in a TMA for immunohistochemical analysis. IHC was carried out for phospho- and total IGF-IR. Representative IHC staining of the treatment groups is taken at 40× magnification. C, representative tumor sections of the treatment groups stained with H&E are taken at 40× magnification. D, quantification of BrdU incorporation per cell was done by image analysis. Data represent means ± standard error (SE) of 12 representative photographs per treatment group. E and F, the percentage of Ki67/CC3-positive cells within the tumor was scored. Values represent the means ± SE of 12 representative photographs per treatment group. D–F, bars with different letters (a, b) are significantly different ($P < 0.05$) by ANOVAs and pairwise comparisons with Holm adjustment for multiple comparisons.

Toxicity associated with BMS-754807

Despite the potent inhibitory activity of BMS-754807 on MC1 TNBC tumorgrafts, minimal toxicity was observed in animals at doses that show significant antitumor activity. Mice treated with docetaxel or BMS-754807 as a single agent lost a maximum of 5% body weight (Supplementary Fig. S4B). Combination therapy with BMS-754807 plus docetaxel resulted in a body weight loss of 15%.

BMS-754807 was developed as a dual IGF-IR/InsR small molecule inhibitor that inhibits IGF-IR and InsR with a similar affinity. Because glucose homeostasis *in vivo* is maintained through insulin-mediated uptake of glucose in skeletal muscle and suppression of glucose production in the liver (46), the effect of BMS-754807 on InsR inhibition was determined. As expected, blood glucose levels remained unaltered in mice treated with chemotherapy. However, mice treated once daily with BMS-754807 alone showed a significant 2-fold increase in glucose levels when compared with vehicle-treated mice (adjusted $P = 0.035$; Supplementary Fig. S4C). Interestingly, mice treated with the combination of BMS-754807 and docetaxel showed a lower elevation in glucose levels, but this was not significantly different compared with vehicle- or docetaxel-treated mice. Blood insulin levels were also monitored in mice after 14 days of treatment. No changes in insulin were observed in chemotherapy-treated mice compared with vehicle-treated mice. However, insulin levels increased from 0.5 to 110 ng/mL after 14 days of treatment with

BMS-754807 alone (adjusted $P < 0.0001$; Supplementary Fig. S4D). Consistent with the reduction in elevated levels of glucose in the combination treatment group, BMS-754807 and chemotherapy induced insulin levels (57ng/mL) to a level lower than BMS-754807 alone (114 ng/mL), which was not significant; however, the hyperinsulinemia produced by the combination treatment was still significantly elevated compared with vehicle or chemotherapy alone (adjusted $P < 0.0001$).

BMS-754807 blocks growth, induces apoptosis, and sensitizes MC1 tumorgrafts to docetaxel-induced mitotic catastrophe

Several reports have shown that chemotherapy agents such as docetaxel affect the stability of the microtubules and in doing so induce mitotic catastrophe (47, 48). Mitotic catastrophe results from aberrant mitosis or mis-segregation of chromosomes followed by cell division, which results in the formation of multinucleated giant cells leading to cell death, which, in turn, through mitotic catastrophe may occur through apoptosis and necrosis (48). MC1 tumorgrafts treated with docetaxel showed relatively few multinucleated giant cells (Fig. 6C). However, the addition of BMS-754807 dramatically increased docetaxel-induced mitotic catastrophe (Fig. 6C). Analysis of hematoxylin and eosin (H&E) staining showed that normal breast cancer cells were still present in docetaxel-treated tumors whereas only multinucleated cells were present in the combination treated tumors.

Because multinucleated cells may be temporarily viable and mitotic catastrophe may be a process leading to death (48), we analyzed treated tumors for replication, proliferation, and apoptosis. All treatment groups showed a reduction in replication, as indicated by less 5-bromo-2-deoxyuridine (BrdU) incorporation into DNA than into untreated tumor cells (Fig. 6D). BMS-754807 alone reduced replication by 36% (22% BrdU-positive cells in vehicle tumors vs. 16% in treated tumors), but this was not significant (adjusted $P = 0.13$). Chemotherapy significantly reduced replication by 55% (adjusted $P = 0.015$) and the combination by 59% compared with vehicle (adjusted $P = 0.0018$). We next analyzed proliferation as assessed by Ki67-positive cells (Fig. 6E; Supplementary Fig. S4D). Whereas both single agents alone could significantly reduce proliferation by 30% to 32% (adjusted $P < 0.0001$), combination treatment resulted in only a 17% reduction in proliferation (adjusted $P < 0.005$, compared with vehicle). We then investigated whether single agents alone or the combination of BMS-754807 and docetaxel induced cell death. BMS-754807 caused a 4-fold elevation in apoptosis as measured by cleaved caspase 3 (CC3) from 3% apoptotic cells in vehicle-treated tumors to 11% in BMS-754807–treated tumors (Fig. 6F; Supplementary Fig S4D); however, this elevation was not significant (adjusted $P = 0.36$). Chemotherapy resulted in a 6.7-fold induction of apoptosis compared with vehicle (adjusted $P = 0.1$), which again was not significant, whereas the combination of BMS-754807 and chemotherapy caused a striking 12-fold induction of apoptosis compared with vehicle-treated tumors (Fig. 6F; Supplementary Fig S4D), which was highly significant (adjusted $P = 0.005$). In addition, combination therapy resulted in massive cell destruction through necrosis, as shown in Figure 6C.

Discussion

An important component in the clinical development of targeted therapies against cancer is to identify appropriate patient populations in which tumors show addiction to a particular pathway for continued survival and proliferation and in which these tumors are susceptible to the drug. In this study, we confirmed that an IGF gene signature could measure IGF activity, based on reversion of the signature in 3 different cancer models treated with different anti–IGF-IR therapies. We found that the majority of human TNBCs and their cell lines have an active IGF signature. Consistent with this, TNBC cells lines are most sensitive to the dual anti–IGF-IR/InsR TKI BMS-754807 and sensitivity correlates with expression of the IGF signature. Finally, new tumorgraft models of TNBC show activation of IGF-IR and treatment with BMS-754807 in combination with chemotherapy results in complete tumor regression. This preclinical study provides a strong clear biological rationale to test anti–IGF-IR therapy in combination with chemotherapy in patients with TNBC.

Although many studies identified ER-positive breast cancer as an important target for anti–IGF-IR therapy, the significance of IGF-IR as a target in TNBC has been poorly addressed. However, there is a growing literature indicating a role for IGF-IR in the aggressive subtype of breast cancer. IGF-IR is amplified (albeit in a small number of tumors) in TNBC (29) and IGF-IR protein is detected in TNBC (30). Moreover, activated (phosphorylated) IGF-IR and InsR are also found in TNBC (18). Growth inhibition of the TNBC cell line SUM149 *in vitro* with BMS-536924 suggests that this subtype of breast cancer may be inhibited by targeting IGF-IR/InsR (18).

There has been recent, considerable interest in the identification of biomarkers for anti–IGF-IR therapies. Several *in vitro* cell culture studies have recently been reported. Studies of an IGF-IR TKI, NVP-AEW541, reported high levels of IGF-IR in all breast cancer cell lines (49). IGF-IR expression alone provided insufficient information to select cell lines sensitive to NVP-AEW541, but sensitivity was limited to those that express both IGF-IR and IRS1 (49). Huang and colleagues examined response to a panel of neuroblastoma and sarcoma cells lines to BMS-536924 and identified genes differentially expressed between sensitive and resistant cell lines. Interestingly, IGF-IR mRNA was a weak predictive marker of response to BMS-536924, but prediction improved when the levels of IGF-IR, IGF-I, and IGF-II were also considered (50). We found that IGF-IR mRNA levels did not predict response to BMS-536924 in breast cancer cell lines but, in contrast, that IGF-IR protein was weakly associated with response (51). Similarly, a study in lung cancer cells

showed that IGF-IR protein predicts response to a monoclonal antibody R1507 (52). A study of a large panel of breast cancer cell lines in response to the monoclonal antibody h10H5 showed that IGF-IR mRNA levels correlate with response, with IGF-IR mRNA being an excellent negative predictive factor (low levels being associated with resistance) but mRNA levels being a relatively poor positive predictive factor. Importantly, inclusion of IGF-II, IRS1, and IRS2 mRNA levels increases the potential to predict which cells respond to h10H5 (53). We recently carried out the first pilot analysis in a phase 2 clinical trial in a small number of human NSCLC tumors treated with the anti–IGF-IR antibody Figitumumab (Pfizer) and found that IGF-IR was a weak predictor of response (54). To date, the majority of data suggest that IGF-IR may be a relatively strong negative predictive factor, similar to the ER for hormone therapy and HER2 for anti-HER2 therapy, but that IGF-IR alone is a weak positive predictive factor. Interestingly, ER seems to be a strong negative predictor of response to BMS-754807 and correlates more with response than the actual IGF signature. This is likely because ER is a major driver of proliferation and survival in many ER-positive cell lines and inhibition of ER would likely sensitize some of these cell lines to an IGF-IR inhibitor. Supporting this, cotreatment with antiestrogen and anti–IGF-IR inhibitors shows additive and synergistic effects both *in vitro* and *in vivo* (55, 56).

We developed the IGF signature to learn more about transcriptional events downstream of IGF-IR and to examine the role of IGF-IR–regulated genes in breast cancer. However, the obvious question as to the potential role of the IGF signature in predicting response to anti–IGF-IR therapy arose. We show here that the IGF gene signature can measure IGF activity in tumors; however, it also measures other related growth factor pathways. Not surprisingly, the IGF signature is only weakly correlated ($r = 0.41$) with response of cells to an IGF-IR inhibitor. However, the strength of the signature may come when used in combination with IGF-IR protein levels and activity. Thus, IGF-IR alone, or the IGF signature alone, may be insufficient to indicate an active IGF pathway, but the combination may better indicate an active IGF pathway. To this end, we used this strategy to select a TNBC tumorgraft for study and found dramatic effects of an IGF-IR inhibitor. Further comprehensive studies are required to definitively prove whether the combination of IGF-IR levels and downstream gene transcripts is a useful method to identify patients who may respond to anti–IGF-IR therapy.

Standard xenografts using permanent cell lines poorly predict how a drug works in patients with the same type of tumor (43). A study showed that tumorgrafts correctly predict response in 90% of patients (19/21 tumors) and resistance in 97% (57/59) of tumors (57). A clinical trial in pediatric neuroblastoma testing the drug topotecan was consistent with that reported in preclinical tumorgraft models of neuroblastoma (58). Therefore, we chose to study recently developed tumorgrafts, in which tumors were taken from patients and small pieces were directly implanted into immunodeficient mice. We found a dramatic effect of BMS-754807 against MC1 tumorgrafts, with complete regression when the drug was combined with chemotherapy. Complete regression of standard cell line xenografts has been rarely reported, and we found that BMS-754807 showed only minimal activity against a range of breast cancer cell lines grown as xenografts (data not shown), again indicating that the tumorgraft model may be more appropriate for determining response.

IGF-IR has been linked to resistance to hormone therapy, anti-HER2 therapy, chemotherapy, and radiation therapy (25). As such, there is great interest in combing anti–IGF-IR therapies with currently anticancer agents. IGF-IR signals to potent survival pathways and has been shown to confer resistance to chemotherapy-induced death (59, 60). Consistent with this, inhibition of the IGF-IR sensitizes breast cancer cells to chemotherapy (61, 62). In this study, we combined BMS-754807 with docetaxel, as it has previously been shown that IGF-IR is a mediator of survival to taxanes and the combination of an IGF-IR antibody (A12) and docetaxel showed excellent antitumor activity in prostate cancer (63). We found a similar effect with the combination therapy. Why anti–IGF-IR therapy is so active in combination with an antimicrotubule therapy is intriguing. As anti-IGF therapy is thought to mainly act as a G_1 block, and docetaxel causes a G_2/M block, it is possible that the double blockade is especially effective. However, a study showed that anti–IGF-IR blockade causes a G_2/M block (63). Indeed, in our analysis of the IGF signature, Ingenuity Pathway Analysis identified G_2/M checkpoint as the major IGF-regulated process after 24 hours, with IGF upregulating numerous genes, including *AURKA*, *AURKB*, *BUB1*, *CCNB*, *CENPE*, *CENPA*, and *CDCA8*, involved in G_2/M transition. Thus, is it possible that IGF-IR normally confers G_2/M progression and that in combination with docetaxel this leads to mitotic catastrophe. However, further intrigue is provided by the finding that BMS-754807 actually inhibits AURKA (31), albeit with lower affinity than IGF-IR. It is thus possible that BMS-754807 and docetaxel synergize due to a concomitant action on the G_2/M checkpoint.

In summary, this preclinical study shows that an IGF-IR/InsR inhibitor is active in TNBC and provides substantial support and rationale for a clinical trial using BMS-754807 in ER-negative and HER2-negative breast cancer.

Disclosure of Potential Conflicts of Interest

B.C. Litzenburger, C.J. Creighton, A. Tsimelzon, B.T. Chan, S.G. Hilsenbeck, T. Wang, J.C. Chang, M.T. Lewis, and A.V. Lee have no conflict of interest. J.M. Carboni, M.M. Gottardis, and F. Huang are employees of Bristol-Myers Squibb.

Acknowledgments

We thank Dr. Max Wicha (University of Michigan Comprehensive Cancer Center, Ann Arbor, MI) for providing the MC1 tumor model and Dr. Melissa Landis, Ricardo Moraes, and Lacey Dobrolecki, and others in the Breast Center at Baylor College of Medicine for technical assistance

and helpful suggestions. We also thank the pathology core at the Lester and Sue Smith Breast Center for IHC staining and Stephen Hillerman at Bristol-Myers Squibb for measuring serum glucose and insulin levels.

Grant Support

The study was supported in part by a research grants from the NIH/National Cancer Institute NIH/NCI R01CA94118 (A.V. Lee), P50CA58183 (A.V. Lee/J.C. Chang/M.T. Lewis), and R01-CA138197 (J.C. Chang /M.T. Lewis). B. Litzenburger is a recipient of the Department of Defense Predoctoral Traineeship Award (DAMD-W81XWH-08-1-0220).

The costs of publication of this article were defrayed in part by the payment of page charges. This article must therefore be hereby marked *advertisement* in accordance with 18 U.S.C. Section 1734 solely to indicate this fact.

Received July 16, 2010; revised November 15, 2010; accepted December 6, 2010; published OnlineFirst December 22, 2010.

References

1. Early Breast Cancer Trialists' Collaborative Group. Effects of chemotherapy and hormonal therapy for early breast cancer on recurrence and 15-year survival: an overview of the randomised trials. Lancet 2005;365:1687–717.
2. Pusztai L. Current status of prognostic profiling in breast cancer. Oncologist 2008;13:350–60.
3. Sørlie T, Perou CM, Tibshirani R, Aas T, Geisler S, Johnsen H, et al. Gene expression patterns of breast carcinomas distinguish tumor subclasses with clinical implications. Proc Natl Acad Sci U S A 2001;98:10869–74.
4. Sørlie T, Tibshirani R, Parker J, Hastie T, Marron JS, Nobel A, et al. Repeated observation of breast tumor subtypes in independent gene expression data sets. Proc Natl Acad Sci U S A 2003;100:8418–23.
5. Kreike B, van Kouwenhove M, Horlings H, Weigelt B, Peterse H, Bartelink H, et al. Gene expression profiling and histopathological characterization of triple-negative/basal-like breast carcinomas. Breast Cancer Res 2007;9:R65.
6. Rakha EA, Tan DS, Foulkes WD, Ellis IO, Tutt A, Nielsen TO, et al. Are triple-negative tumours and basal-like breast cancer synonymous?- Breast Cancer Res 2007;9:404.
7. Rakha E, Reis-Filho J, Ellis I. Basal-like breast cancer: a critical review. J Clin Oncol 2008;26:2568–81.
8. Cleator S, Heller W, Coombes RC. Triple-negative breast cancer: therapeutic options. Lancet Oncol 2007;8:235–44.
9. Carey LA, Perou CM, Livasy CA, Dressler LG, Cowan D, Conway K, et al. Race, breast cancer subtypes, and survival in the Carolina Breast Cancer Study. JAMA 2006;295:2492–502.
10. Pollak MN, Schernhammer ES, Hankinson SE. Insulin-like growth factors and neoplasia. Nat Rev Cancer 2004;4:505–18.
11. Kurmasheva RT, Houghton PJ. IGF-I mediated survival pathways in normal and malignant cells. Biochim Biophys Acta 2006;1766:1–22.
12. Carboni JM, Lee AV, Hadsell DL, Rowley BR, Lee FY, Bol DK, et al. Tumor development by transgenic expression of a constitutively active insulin-like growth factor I receptor. Cancer Res 2005;65:3781–7.
13. Jones HE, Lippman SA, Pinho AA, Luppi CG, van de Wijgert JH, Diaz J, et al. Transgenic overexpression of IGF-IR disrupts mammary ductal morphogenesis and induces tumor formation. Oncogene 2007;26:1636–44.
14. Irie HY, Pearline RV, Grueneberg D, Hsia M, Ravichandran P, Kothari N, et al. Distinct roles of Akt1 and Akt2 in regulating cell migration and epithelial-mesenchymal transition. J Cell Biol 2005;171:1023–34.
15. Kim HJ, Litzenburger BC, Cui X, Delgado DA, Grabiner BC, Lin X, et al. Constitutively active IGF-IR causes transformation and xenograft growth of immortalized mammary epithelial cells, and is accompanied by an epithelial to mesenchymal transition mediated by NF-kappaB and Snail. Mol Cell Biol 2007;27:3165–75.
16. Yanochko GM, Eckhart W. Type I insulin-like growth factor receptor over-expression induces proliferation and anti-apoptotic signaling in a three-dimensional culture model of breast epithelial cells. Breast Cancer Res 2006;8:R18.
17. Resnik JL, Reichart DB, Huey K, Webster NJ, Seely BL. Elevated insulin-like growth factor I receptor autophosphorylation and kinase activity in human breast cancer. Cancer Res 1998;58:1159–64.
18. Law JH, Habibi G, Hu K, Masoudi H, Wang MY, Stratford AL, et al. Phosphorylated insulin-like growth factor-i/insulin receptor is present in all breast cancer subtypes and is related to poor survival. Cancer Res 2008;68:10238–46.
19. Key TJ, Appleby PN, Reeves GK, Roddam AW. Insulin-like growth factor 1 (IGF1), IGF binding protein 3 (IGFBP3), and breast cancer risk: pooled individual data analysis of 17 prospective studies. Lancet Oncol ;11:530–42.
20. Haluska P, Shaw HM, Batzel GN, Yin D, Molina JR, Molife LR, et al. Phase I dose escalation study of the anti insulin-like growth factor-I receptor monoclonal antibody CP-751,871 in patients with refractory solid tumors. Clin Cancer Res 2007;13:5834–40.
21. Karp DD, Paz-Ares LG, Novello S, Haluska P, Garland L, Cardenal F, et al. Phase II study of the anti-insulin-like growth factor type 1 receptor antibody CP-751,871 in combination with paclitaxel and carboplatin in previously untreated, locally advanced, or metastatic non-small-cell lung cancer. J Clin Oncol 2009;27:2516–22.
22. Sachdev D, Yee D. Disrupting insulin-like growth factor signaling as a potential cancer therapy. Mol Cancer Ther 2007;6:1–12.
23. Lee AV, Jackson JG, Gooch JL, Hilsenbeck SG, Coronado-Heinsohn E, Osborne CK, et al. Enhancement of insulin-like growth factor signaling in human breast cancer: estrogen regulation of insulin receptor substrate-1 expression *in vitro* and *in vivo*. Mol Endocrinol 1999;13:787–96.
24. Lee AV, Weng CN, Jackson JG, Yee D. Activation of estrogen receptor-mediated gene transcription by IGF-I in human breast cancer cells. J Endocrinol 1997;152:39–47.
25. Casa AJ, Dearth RK, Litzenburger BC, Lee AV, Cui X. The type I insulin-like growth factor receptor pathway: a key player in cancer therapeutic resistance. Front Biosci 2008;13:3273–87.
26. Sachdev D, Yee D. Inhibitors of insulin-like growth factor signaling: a therapeutic approach for breast cancer. J Mammary Gland Biol Neoplasia 2006;11:27–39.
27. Weroha S, Haluska P. IGF-1 Receptor inhibitors in clinical trials—early lessons. J Mammary Gland Biol Neoplasia 2008;13:471–83.
28. Sarfstein R, Maor S, Reizner N, Abramovitch S, Werner H. Transcriptional regulation of the insulin-like growth factor-I receptor gene in breast cancer. Mol Cell Endocrinol 2006;252:241–6.
29. Adélaïde J, Finetti P, Bekhouche I, Repellini L, Geneix J, Sircoulomb F, et al. Integrated profiling of basal and luminal breast cancers. Cancer Res 2007;67:11565–75.
30. Lerma E, Peiro G, Ramon T, Fernandez S, Martinez D, Pons C, et al. Immunohistochemical heterogeneity of breast carcinomas negative for estrogen receptors, progesterone receptors and Her2//neu (basal-like breast carcinomas). Mod Pathol 2007;20:1200–7.
31. Carboni JM, Wittman M, Yang Z, Lee F, Greer A, Hurlburt W, et al. BMS-754807, a small molecule inhibitor of insulin-like growth factor-1R/IR. Mol Cancer Ther 2009;8:3341–9.
32. Neve RM, Chin K, Fridlyand J, Yeh J, Baehner FL, Fevr T, et al. A collection of breast cancer cell lines for the study of functionally distinct cancer subtypes. Cancer Cell 2006;10:515–27.
33. Li C, Wong WH. Model-based analysis of oligonucleotide arrays: expression index computation and outlier detection. Proc Natl Acad Sci U S A 2001;98:31–6.
34. Li C, Hung Wong W. Model-based analysis of oligonucleotide arrays: model validation, design issues and standard error application. Genome Biol 2001;2:RESEARCH0032.
35. Hoadley K, Weigman V, Fan C, Sawyer LR, He X, Troester MA, et al. EGFR associated expression profiles vary with breast tumor subtype. BMC Genom 2007;8:258.

36. Creighton CJ, Casa A, Lazard Z, Huang S, Tsimelzon A, Hilsenbeck SG, et al. Insulin-like growth factor-I activates gene transcription programs strongly associated with poor breast cancer prognosis. J Clin Oncol 2008;26:4078–85.
37. Creighton CJ, Li X, Landis M, Dixon JM, Neumeister VM, Sjolund A, et al. Residual breast cancers after conventional therapy display mesenchymal as well as tumor-initiating features. Proc Natl Acad Sci U S A 2009;106:13820–5.
38. Desmedt C, Piette F, Loi S, Wang Y, Lallemand F, Haibe-Kains B, et al. Strong time dependence of the 76-gene prognostic signature for node-negative breast cancer patients in the TRANSBIG multicenter independent validation series. Clin Cancer Res 2007;13:3207–14.
39. Shang Y, Mao Y, Batson J, Scales SJ, Phillips G, Lackner MR, et al. Antixenograft tumor activity of a humanized anti-insulin-like growth factor-I receptor monoclonal antibody is associated with decreased AKT activation and glucose uptake. Mol Cancer Ther 2008;7:2599–608.
40. Pappano WN, Jung PM, Meulbroek JA, Wang YC, Hubbard RD, Zhang Q, et al. Reversal of oncogene transformation and suppression of tumor growth by the novel IGF1R kinase inhibitor A-928605. BMC Cancer 2009;9:314.
41. Whitfield ML, Sherlock G, Saldanha AJ, Murray JI, Ball CA, Alexander KE, et al. Identification of genes periodically expressed in the human cell cycle and their expression in tumors. Mol Biol Cell 2002;13:1977–2000.
42. Loboda A, Nebozhyn M, Cheng C, Vessey R, Huang P, Dai H, et al. Biomarker discovery: identification of a growth factor gene signature. Clin Pharmacol Ther 2009;86:92–6.
43. Garber K. From human to mouse and back: "tumorgraft" models surge in popularity. J Natl Cancer Inst 2009;101:6–8.
44. Ginestier C, Hur MH, Charafe-Jauffret E, Monville F, Dutcher J, Brown M, et al. ALDH1 is a marker of normal and malignant human mammary stem cells and a predictor of poor clinical outcome. Cell Stem Cell 2007;1:555–67.
45. Zeng X, Sachdev D, Zhang H, Gaillard-Kelly M, Yee D. Sequencing of type I insulin-like growth factor receptor inhibition affects chemotherapy response *in vitro* and *in vivo*. Clin Cancer Res 2009;15:2840–9.
46. Leney SE, Tavare JM. The molecular basis of insulin-stimulated glucose uptake: signalling, trafficking and potential drug targets. J Endocrinol 2009;203:1–18.
47. Morse DL, Gray H, Payne CM, Gillies RJ. Docetaxel induces cell death through mitotic catastrophe in human breast cancer cells. Mol Cancer Ther 2005;4:1495–504.
48. Vakifahmetoglu H, Olsson M, Zhivotovsky B. Death through a tragedy: mitotic catastrophe. Cell Death Differ 2008;15:1153–62.
49. Mukohara T, Shimada H, Ogasawara N, Wanikawa R, Shimomura M, Nakatsura T, et al. Sensitivity of breast cancer cell lines to the novel insulin-like growth factor-1 receptor (IGF-1R) inhibitor NVP-AEW541 is dependent on the level of IRS-1 expression. Cancer Lett 2009; 282:14–24.
50. Huang F, Greer A, Hurlburt W, Han X, Hafezi R, Wittenberg GM, et al. The mechanisms of differential sensitivity to an insulin-like growth factor-1 receptor inhibitor (BMS-536924) and rationale for combining with EGFR/HER2 inhibitors. Cancer Res 2009;69:161–70.
51. Litzenburger BC, Kim HJ, Kuiatse I, Carboni JM, Attar RM, Gottardis MM, et al. BMS-536924 reverses IGF-IR-induced transformation of mammary epithelial cells and causes growth inhibition and polarization of MCF7 cells. Clin Cancer Res 2009;15:226–37.
52. Gong Y, Yao E, Shen R, Goel A, Arcila M, Teruya-Feldstein J, et al. High expression levels of total IGF-1R and sensitivity of NSCLC cells *in vitro* to an anti-IGF-1R antibody (R1507). PLoS One 2009;4:e7273.
53. Zha J, O'Brien C, Savage H, Huw LY, Zhong F, Berry L, et al. Molecular predictors of response to a humanized anti–insulin-like growth factor-I receptor monoclonal antibody in breast and colorectal cancer. Mol Cancer Ther 2009;8:2110–21.
54. Gualberto A, Dolled-Filhart M, Gustavson M, Christiansen J, Wang YF, Hixon ML, et al. Molecular analysis of non-small cell lung cancer identifies subsets with different sensitivity to insulin-like growth factor I receptor inhibition. Clin Cancer Res 2010;16:4654–65.
55. Lisztwan J, Pornon A, Chen B, Chen S, Evans DB. The aromatase inhibitor letrozole and inhibitors of insulin-like growth factor I receptor synergistically induce apoptosis in *in vitro* models of estrogen-dependent breast cancer. Breast Cancer Res 2008;10:R56.
56. Cohen BD, Baker DA, Soderstrom C, Tkalcevic G, Rossi AM, Miller PE, et al. Combination therapy enhances the inhibition of tumor growth with the fully human anti-type 1 insulin-like growth factor receptor monoclonal antibody CP-751,871. Clin Cancer Res 2005;11:2063–73.
57. Fiebig HH. 13 Patient and cell line derived human tumor xenograft models—preclinical/clinical correlationsEur J Cancer 2004;2:8.
58. Santana VM, Furman WL, Billups CA, Hoffer F, Davidoff AM, Houghton PJ, et al. Improved response in high-risk neuroblastoma with protracted topotecan administration using a pharmacokinetically guided dosing approach. J Clin Oncol 2005;23:4039–47.
59. Gooch JL, Van Den Berg CL, Yee D. Insulin-like growth factor (IGF)-I rescues breast cancer cells from chemotherapy-induced cell death–proliferative and anti-apoptotic effects. Breast Cancer Res Treat 1999;56:1–10.
60. Miglietta A, Panno ML, Bozzo F, Gabriel L, Bocca C. Insulin can modulate MCF-7 cell response to paclitaxel. Cancer Lett 2004; 209:139–45.
61. Fowler CA, Perks CM, Newcomb PV, Savage PB, Farndon JR, Holly JM. Insulin-like growth factor binding protein-3 (IGFBP-3) potentiates paclitaxel-induced apoptosis in human breast cancer cells. Int J Cancer 2000;88:448–53.
62. Beech DJ, Parekh N, Pang Y. Insulin-like growth factor-I receptor antagonism results in increased cytotoxicity of breast cancer cells to doxorubicin and taxol. Oncol Rep 2001;8:325–9.
63. Wu JD, Haugk K, Coleman I, Woodke L, Vessella R, Nelson P, et al. Combined *in vivo* effect of A12, a type 1 insulin-like growth factor receptor antibody, and docetaxel against prostate cancer tumors. Clin Cancer Res 2006;12:6153–60.